Journal of Mining and Environment (JME) Vol. 15, No. 3, 2024, 1051-1070

Shahrood University of Technology

Journal of Mining and Environment (JME)

Journal homepage: www.jme.shahroodut.ac.ir

Iranian Society of Mining Engineering (IRSME)

On 2D Discrete Element Analyses of Transversely Isotropic Elastic Geo-materials; Insight to Scale Effects and Loading Rate

Vahab Sarfarazi[1], Hadi Haeri[2*], Mohammad Fatehi Marji[3], and Gholamreza Saeedi[4]

1. Department of Mining Engineering, Hamedan University of Technology, Hamedan, Iran
2. Department of Mining Engineering, Higher Education Complex of Zarand, Shahid Bahonar University of Kerman, Kerman, Iran
3. Department of Mining and Metallurgical Engineering, Yazd University, Yazd, Iran
4. Department of Mining Engineering, Shahid Bahonar University of Kerman, Kerman, Iran

Article Info

Received 30 August 2023

Received in Revised form 17 December 2023

Accepted 30 December 2023

Published online 30 December 2023

DOI: 10.22044/jme.2023.13538.2502

Keywords

Bedding layer

Intersection plane

Conventional strength tests

Discrete element

Layer inclination angle

Abstract

The mechanical behaviour of transversely isotropic elastic rocks can be numerically simulated by the discrete element method. The successive bedding layers in these rocks may have different mechanical properties. The aim of this research work is to investigate numerically the effect of anisotropy on the tensile behaviour of transversely isotropic rocks. Therefore, the numerical simulation procedure should be well-calibrated by using the conventional laboratory tests, i.e. tensile (Brazilian), uniaxial, and triaxial compression tests. In this study, two transversely isotropic layers were considered in 72 circular models. These models were prepared with the diameter of 54 mm to investigate the anisotropic effects of the bedding layers on the mechanical behaviour of brittle geo-materials. All these layers were mutually perpendicular in the simulated models, which contained three pairs of thicknesses 5 mm/10 mm, 10 mm/10 mm, and 20 mm/10 mm. Three different diameters for models were chosen, i.e. 5 cm, 10 cm, and 15 cm. These samples were subjected under two different loading rates, i.e. 0.01 mm/min and 10 mm/min. The results gained from these numerically simulated models showed that in the weak layers, the shear cracks with the inclination angles 0° to 90° were developed (considering 15° increment). Also, there was no change in the number of shear cracks as the layer thickness was increased. Some tensile cracks were also induced in the intact material of the models. There was no failure in the interface plane toward the layer of higher strength in this research work. The branching was increased by increasing the loading rate. Also, the model strength was decreased by increasing the model scale.

1. Introduction

The problem of heterogeneity on the mechanical behaviour of rock masses is of main concern in the proper design of many surface and underground rock structures used in modern society. Heterogeneity is an intrinsic rock mass property related to the discontinuities and weak planes such as faults, joints, random fractures, pores, and defects and bedding layers. These weaknesses are presented naturally or induced artificially during the formation or disintegration and fragmentation processes in rocks, respectively [1-8]. As far as the rocks discontinuities are concerned, their effects on the tensile, shear, and compressive behaviours of rock masses should be studied individually or in a mixed mode because rocks are relatively weaker under tension and shear loading conditions compared to that of the compression. Therefore, many investigations carried out to study the effects of anisotropy on the tensile behaviour of rock masses encountered in geo-mechanics. The rocks' tensile strengths are mainly measured experimentally in the laboratory by performing the standard indirect tensile strength tests mostly use the Brazilian disc type rocks' specimens under compression [9-17].

Investigation of the tensile behavior of transversely isotropic rocks with intersected layers is very complicated due to difficulty in physical

Corresponding author: haerihadi@gmail.com (H. Haeri)

sample preparation. Therefore, a huge ambiguous exist due to deficiency in researches in this filed. For example, Tien *et al*. [18] investigates the mechanical properties of artificial transversely isotropic rock containing parallel layers (Figure 1). Also, You and Sun [19] study only the influence of bedding plane on mechanical behaviour of surrounding rock in mountain tunnelling (Figure 1b).

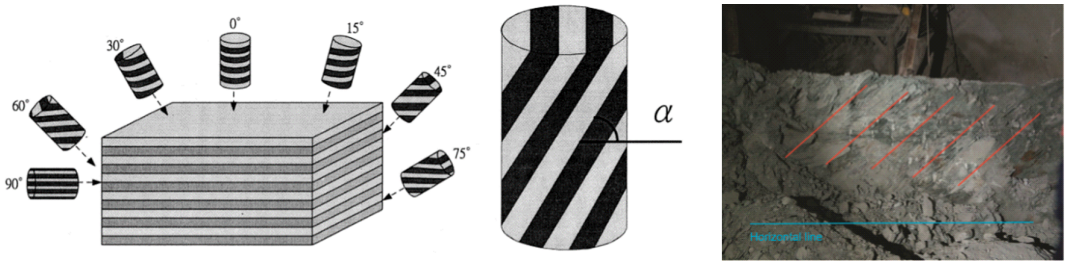

(a) (b)

Figure 1. a) Drilling direction for taking specimens with different dip angles [18], b) Bedding structure of surrounding rock of Xiangli Expressway Tunnel in the Yunnan Province [19].

The Brazilian tensile strength tests on the bedded rock specimens of dolostone performed by Wu *et al*. [20] to consider the effects of anisotropy. The same experiments were performed by other researchers on various rock samples of shale, schist and gneiss, coal, sandstone [21-25]. All these researchers claimed the profound effects of anisotropy on the tensile behaviour of various rock samples.

These studies showed that most of the rock disc samples were failed diametrically irrespective of the weakness planes' directions. However, the induced crack lengths and the fracture patterns at failure varies for different rocks' samples. It means that the inclination angles of discontinuities and their lengths affect the tensile behaviour of rocks [25]. Two tensile failures were observed in the failed samples of rocks based on the layers' inclination angles.

For the relatively low angles (< 60°), the fracture patterns involve the cracks' growth paths parallel to the loading directions, so that there may be no crack branching phenomena and the tensile cracks are mostly independent of the rock laminations. On the other hand, for the bedding layers of high inclination angles (> 60°), the failure mode highly depends on the rocks lamination angles. In some more recent works, Ma *et al*. [26, 27] worked on the anisotropy effects on the rocks' tensile strengths considering the influence of fracture stress in the Brazilian discs. Zhang *et al*. [17] used the acoustic emission (AE) to elucidate the effects of anisotropy on the discs of layered shale in the Brazilian tensile strength tests. The fractures related to the spatial distribution of AE were discussed in the layered rock discs, and explained the failure mechanism due to rocks' anisotropy considering the inclination angles of the bedding planes. The tensile, compressive, and shear strengths of geo-materials highly depends on the fracture trend and failure mode during the loading process as explained by many researchers [28-47].

On the other hand, as far as the bedded rocks are concerned, their behaviours have been studied mainly based on the concept of transversely isotropic behaviour for both the tensile and compressive strengths. The effects of bedding angles and other discontinuities like the natural joints and fractures have been considered too [38, 49]. For example, a high tensile strength (about four times) of a bedded rock was observed when loaded perpendicular to the layers compared to that of the rock loaded parallel to the bedding plane. Many numerical analyses were also performed to study the effects of bedding layers' behaviours on the stability of the underground and surface excavations in jointed and bedded rock masses [3, 29, 50]. Their works were compared with the case studies reported in the literature and found that their results are in consistent with the experimental and field observations [51]. Some experimental tests were also accomplished to study the behaviours of bedded rocks in laboratory [52, 53].

The mechanical characteristics of shale considering the acoustic emission (AE) and tensile strength were investigated by Zhang *et al*. [17]. The effects of laminations' orientations (with respect to the direction of loading) on the behaviour, strength, and damage mechanism of the shale using the Brazilian tensile strength test and AE technics were discussed. Their works can be used for monitoring

the micro-cracking mechanism, rock mass instability, and sequences of earthquakes. Some experimental tests such as direct shear tests were carried out on the stratified and layered rock specimens by Wang *et al*. [11]. The rock specimens were specially prepared from the granulite rocks to be able to measure the effects of directionality and anisotropy of rocks on their shear strengths. Some numerical simulation models were carried out using discrete element method and discrete fracture network (DFN) algorithm to complete their research. Wang *et al*. [54] used the AE technics to analyse the energy release characteristics and the tensile strength of laminated rocks considering the theory of transversely isotropic behaviour for the brittle materials. The results indicated that the AE characteristics and layer orientations (with respect to the loading direction) considerably affect the tensile strength and mechanical behaviour of the laminated rock samples.

A fracture pressure model for the stability analyses of inclined wells in layered rocks was proposed by Ma *et al*. [27]. The effects of bedding planes and their orientation, anisotropy ratio, *in situ* stresses, pore pressure, and the direction of wells on fracture pressure were investigated in their studies. The results showed that the effect of rock anisotropy on the stability of wells is relatively high, and cannot be ignored in rock drilling projects. The aim of the work is to perform a robust numerical investigation on the tensile behaviour of transversely isotropic rocks by considering the effect of anisotropy (i.e. the bedding layers' intersection). The versatile discrete element method code in two dimensions (PFC2D) has been used to perform the numerical analyses.

2. Numerical Modelling with Particle Flow Code (PFC)

The versatile softwares of discrete element methods such as the particle flow code for solving two dimensional problems (PFC2D) in geo-mechanics can be used to simulate the transversely isotropic bedded rocks. A particle assembly is modelled in PFC2D to represent the geo-material sample as circular discs. The planar walls and the contact bonds are considered to generate a sound confined assembly of geo-material particles. The contact and parallel bonded models are prescribed in PFC2D for modelling the particle assemblies of geo-material samples. The physical behaviour of a contact model is assumed to be small and ignorable, so that it can be recognized as a parallel bond of zero radius. On the other hand, in the parallel bond models, a small bond radius in between the rigid particles is considered, so that the shear and normal stiffness can be defined for it. The parallel bonds can also resist the bending moments, while the contact bonds can only withstand the forces acting at the contact points of the particle assembly. Therefore, the tensile and shear strengths at the contact bonds are specified to bear the corresponding forces that may exist at these bonds till exceed the bonding strengths between the particles in the assembly [55.56]. However, the mechanical behaviour and failure mechanisms of the real material samples can be studied effectively by their proper modelling with PFC2D and adopting some appropriately calibrated micro-parameters adjusted based on the experimental macroscopic values obtained from the laboratory tests. The main micro-parameters used for PFC modelling of the geo-material specimens include the elastic modulus and friction coefficient of the contact points between the particles in the assembly, the ratio of normal and shear stiffnesses, the normal and shear strengths, and the minimum radius of the balls. The standard deviation of these parameters together with the parallel bond modulus, its multiplier and its stiffness ratio should also be defined for the parallel bond modelling of the particles as used in this study. However, these micro-parameters are calibrated based on the procedure proposed by Potyondy [56]. The Mohr-Coulomb criterion is used in PFC as the default failure criterion, and is employed in this study. The shear failure of the bonds at the interfaces of the particles may take place when the induced shear stresses between the neighbouring particles exceeds their shear strengths. The bonding shear strengths are related to the friction angle and cohesion of the relative bonds in the particle assembly. The tensile or primary wing cracks may be initiated in the geo-material samples when the induced normal tensile stress super-pass that of the tensile strength of the particle's interfaces. Considering a small dynamic movement of the particles, then each tensile crack extension may generate a small oscillation or wave in the modelled assembly. Adapting a suitable damping coefficient for the model, this seismic wave may attenuate under static conditions. This phenomenon may affect the damping wave, normal, and shear stresses induced in the bonded particles. The process is repeated in a cyclic manner for re-evaluating the failure phenomenon based on the Mohr-Coulomb criterion.

The linear and non-linear models of contacts are used to simulate the particles' frictional sliding and

relative movements of the particles at the contact points in the particle assembly. The relative movements and the resultant contact forces at the contact points are considered to be related to one another by considering the linear elastic behaviour of the modelled geo-material samples at the contact interfaces of their particles. In the discrete formulation of the constitutive equations, it is assumed that the forces and displacements are elastically related to one another. Then some adjusted and calibrated micro-parameters are defined based on the real mechanical characteristics measured in the laboratory testing of the real geo-material specimens. The suitable mechanical micro-properties for the particle assembly modelled in PFC can be estimated by calibrating these parameters versus the actual macro-mechanical parameters measured through the experimental test. The trial-and-error approach based on an inversion solution method is adopted in PFC to calibrate the proper micro-parameters for the modelled assemblies of the particles representing the geo-material samples. This calibration procedure has been stablished and suggested by ITASCA [55].

However, the calibrated material properties are used to model the geo-material specimens in form of particle assemblies using the parallel bon models as originally stablished and proposed by ITASCA [55]. Then main micro-parameters required for modelling the geo-material specimens in the two-dimension particle flow code (PFC2D) include the elastic modulus for the ball-to-ball contacts, the normal and shear strengths for the parallel bonds, the stiffness ratio Kn/Ks for the contact interfaces. The frictional coefficients of the balls, the smallest ball radius, the standard deviation for the normal-shear strengths ratio, the stiffness ration of the parallel bonds, and the radius multiplier.

In this research work, the parallel bond model is used to accurately simulate the mechanical characteristics of the layered geo-materials' specimens. The flat joint model (FJM) and the smooth joint model (SJM) are not suitable for modelling the layered rocks' specimens. These two models are mostly suitable for the jointed rocks which may contain the pre-existing closed cracks.

The particles in the particle assembly of the geo-material specimens modelled in the Particle Flow Code (PFC), and can move in normal and tangential directions. They also have the ability to rotate when they are activated by applying the loads and torques to the geo-material specimens. The shearing and rotational movements of the particles at the contact points during the activation process have the capacity and relative strengths to bear the torque induced at the interfaces of the particles. The contact surfaces modelled by parallel bonds (PBs) are illustrated in Figure 2. The relative stiffness of the bonds and contact surfaces are given, and the bands in the particle assembly may fail in all cases even when the particles are separated from one another. The effectiveness of the PB models for failure and damage characteristics of geo-material specimens modelled by choosing the appropriate micro-parameters and particle assemblies in PFC. In this research work, two distinct contact models, i.e. ball-wall facets and ball-ball points are introduced and used with appropriate assigned micro-parameters to simulate the Brazilian and uniaxial compression tests that usually conducted on geo-material specimens.

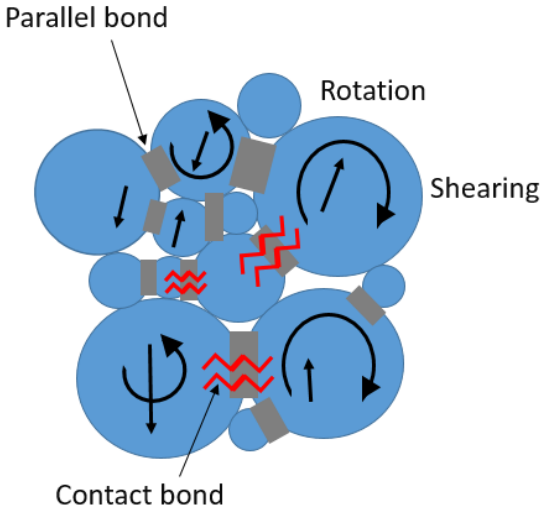

Figure 2. Parallel bond model (PB model).

2.1. Preparing and calibrating numerical model

The proper particle assembly with the calibrated micro-parameters is prepared based on the standard procedures described by Itasca [55] and Potyondy [56]. The four basic steps include: i) particle assembly generation, ii) particle packing, iii) stress initialization for the assembly, and iv) installing the bonds and removing the floating particles from the assembly. In this modelling technique, the gravitational effects of the particles in the assembly are ignored because it may not affect the behaviour of real material samples. In the present work, three experimental tests, i.e. the Brazilian tensile strength and the uniaxial and biaxial compressive tests are carried out in the laboratory on real material samples and the appropriate micro-parameters for calibrating the required particle assemblies are provided based on the trial and error procedure used in the PFC2D modelling of the geo-material samples. Of course, in these tests, the rates of applied loading should be kept low enough to provide the quasi-static condition for the specimens and models. Therefore, the effects of loading rate on the behaviour of the samples, i.e. on the axial stress-axial and lateral strain curves are given in Figure 3 considering two loading rates 0.016 m/s and 0.4 m/s. In the elastic range, the mechanical behaviours of the modelled samples (with 14298 particles in the assembly) do not much depend on the loading rate. As shown in Figure 3, after the elastic limit, there is an oscillatory condition in the mechanical behaviour of the material at high loading rates (0.4 m/s). Therefore, in this research work, the loading rate is fixed as 0.016 m/s. The micro-properties listed in Table 1 (based on standard calibration procedures [56]) are used for calibration in the PFC particle assembly.

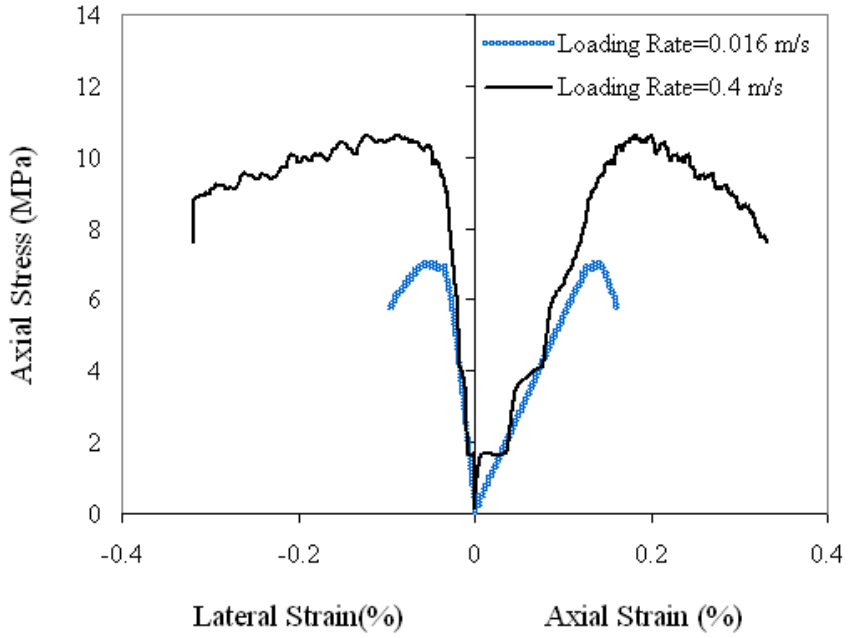

Figure 3. Effects of loading rate on the curves of axial stress versus axial and lateral strains.

Table 1. Micro-properties used to represent intact rock.

Parameters	Values	Parameters	Values
Type of particles	Disc	Parallel-bond radius multiplier	1
Density (kg/m^3)	1000	Young's modulus of parallel bond (GPa)	4
Minimum radius (mm)	0.27	Parallel bond stiffness ratio	1.7
Size ratio	1.56	Particle friction coefficient	0.4
porosity	0.08	Parallel bond normal strength, mean (MPa)	5.6
Damping ratio	0.7	Parallel bond normal strength, std. dev. (MPa)	1.4
Contact Young's modulus (GPa)	4	Parallel bond shear strength, mean (MPa)	5.6
Stiffness ratio	1.7	Parallel bond shear strength, std. dev. (MPa)	1.4

In the numerical model, the stiffness ratios of contacts and parallel bonds control the Poisson's ratio of the assembly. The stiffness ratio of parallel bonds mainly affects the mechanical characteristics of the matrix bonding the particles, and the contact stiffness ration largely affects the contacts' mechanical behavior of the particles. For the similar values of the stiffness ratios, the contacts and parallel bonds (cementations) are the same. In the concrete specimens, the low value of Poisson's ratio demonstrates that the lateral strain is much lower than the axial strain. The same phenomenon is true for the crystalline rocks with rare cementation in between the particles. The homogeneity of the crystalline rocks demonstrates that the both contact and parallel bond stiffness ratios are the same in the numerical models. However, the calibration of models decreases for the homogeneous concrete and rock specimens.

2.1.1. Numerical unconfined compressive test

The numerically simulated test for unconfined compressive strength of the sample is depicted In Figures 4. In these figures, the black and red lines demonstrate the tensile and shear failures in the model, respectively. The sample is modelled by moving the side walls of the sample toward each other to compress the particles in the assembly (Figure 4a). The sample's walls are assumed to be frictionless and rigid. The total number of particles is 14298 for a specimen of 54 mm in diameter and 108 mm in height. However, the range particle size in the model (considering the radii of the particles) is from 0.27 to 0.4212 mm. The bonds in between the particles are kept as small as possible. Of course, there is some limitations as far as the computational efficiency and running time are concerned. For a relatively dense packed assembly, a porosity ratio of 0.08 seems reasonable for this modelling work. However, the calibrated Young modulus, Poisson's ratio, unconfined compressive strength, and crack initiation stresses can be gained from PFC2D models [56]. As shown in Figure 4b, a relatively vertical failure plane is obtained from the numerical simulation observed from the corresponding experimental test.

The numerically simulated values of the mechanical properties of the samples are compared with their experimentally measured counterparts in Table 2.

Table 2. Macro-mechanical properties of model material in experimental test and PFC2D.

Mechanical properties	Experimental results	PFC2D model results
Elastic modulus (GPa)	5	5
Poisson's ration,	0.18	0.19
UCS (MPa)	6.6	6.7
Crack initiation stress (MPa)	3.2	3.2
Brazilian tensile strength$_t$ (MPa)	1	1.1
Friction angle	20.4	21
Cohesion (MPa)	2.2	2.2

2.1.2. Brazilian test

To calibrate the PFC2D model based on the Brazilian tensile strength test, some disc type models of 54 mm in diameter and 27 mm in height with a total number of 5615 particles were prepared. Then a loading rate of 0.016 m/s was applied to crush the lateral walls of the assembly. Figures 4c and 4d demonstrate the failure and fracturing patterns of the numerically modelled samples and experimental tested specimens, respectively. As it can be deduced from the comparison of these figures, the numerical results are very close to those of the experimental observations. Figure 4e demonstrate the tensile behaviour of the samples (i.e. the diagram of axial stress versus the strains). As shown in this figure, the brittle behaviour of the geo-material samples can be easily modelled by PFC2D. However, the numerically approximated tensile strengths of the modelled samples are compared with those gained from the experimental tests in Table 2.

2.1.3. Biaxial test

The biaxial tests were also accomplished on the geo-material samples, and simultaneously some PFC models were also analysed. The biaxial testing samples were modelled in a rectangular shape and loaded from four sides. The top and bottom walls served as the platens for incremental loading at a rate of 0.016 m/s, and the lateral walls were kept at a constant confinement during the testing period. The normal stiffness of the lateral walls was selected as a fraction (i.e. 0.001-0.2) of the average normal stiffness of the particles. In the experimental testing, the vertical loads are applied to the top and bottom surfaces at a specified loading rate (0.016 m/s). The lateral loads are applied by a servo-mechanism, which controls to exert a

constant loading on the four sides of the specimen. For the biaxial loading case, the strengths envelopes for the PFC modelled samples and the experimentally tested geo-material are given in Figure 4f. It has been shown that the predicted biaxial behaviours of the modelled samples by PFC2D are exactly the same as those observed in the experimental biaxial testing in the laboratory.

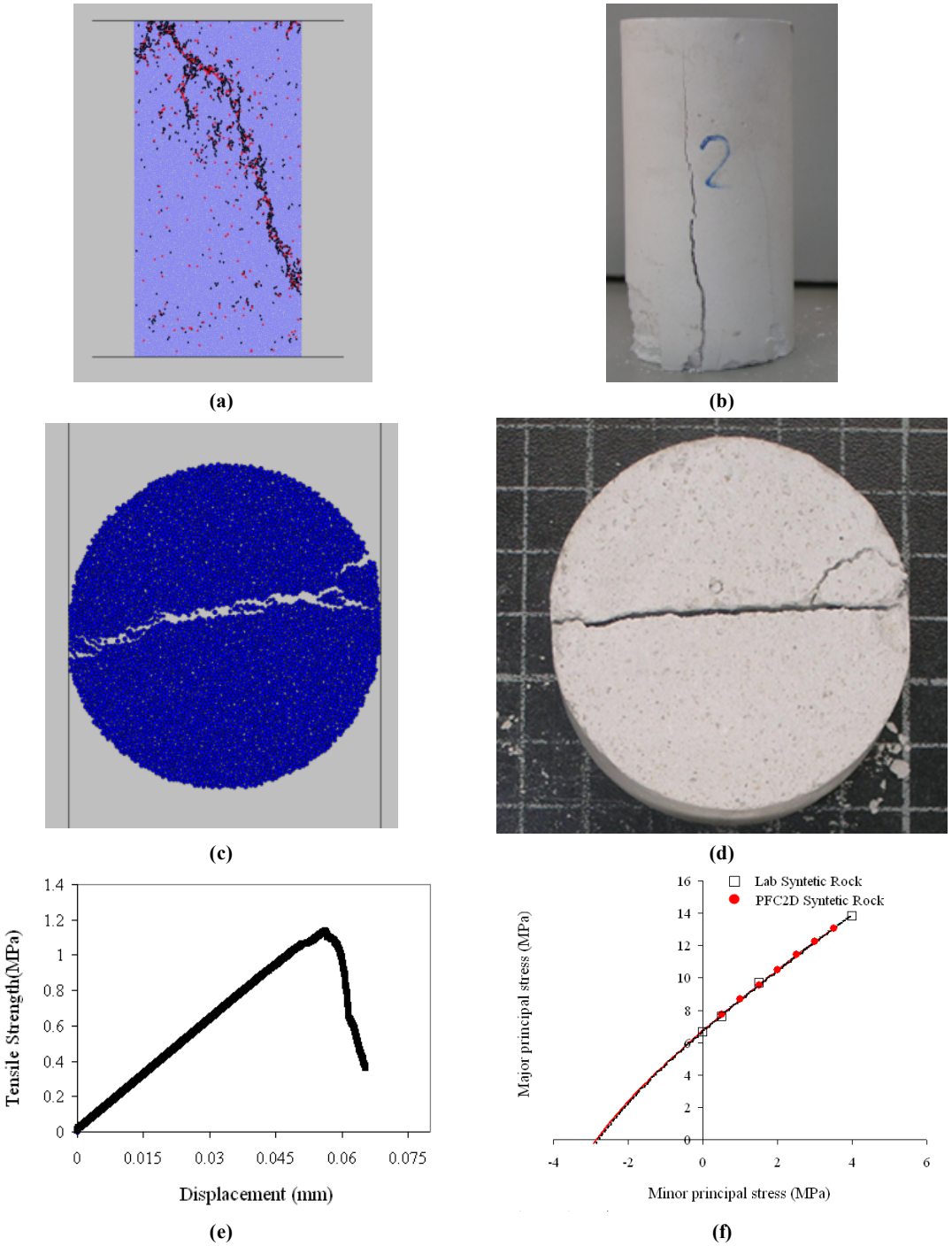

Figure 4. The compressive and tensile behaviour of the geo-material specimens: a) The unconfined compressive test (tensile and shear cracks in the specimens are described by red and black lines, respectively), b) The failure mechanisms in the physical uniaxial samples, c) The failure mechanism of the specimens modelled numerically in PFC2D, d) The failure mechanism in the real (physical) Brazilian disc type samples, e) Tensile strength versus axial displacement curve for the numerically simulated Brazilian test, f) The calibrated failure locus for the PFC2D model of the synthetic rock samples, as compared to that observed from the laboratory test.

2.2. Numerical uniaxial test on non-persistent open joint

2.2.1. Preparing model

The transversely isotropic bedded rock samples can be effectively modelled by PFC2D after its calibration (as explained in the previous sections).

The Brazilian tests on disc type samples consist of two layers with or without cracks (joints) are numerically modelled based on the calibrated micro-parameters, as shown in Figures 5-7. The modelled Brazilian disc type samples are of diameter 54 mm and height of 27 mm and about 81179 particles of radius 0.27 mm are used to prepare the assembly representing the bedded specimens. The particle assembly has two loading walls with two unparalleled bedding layers to represent the transversely isotropic conditions of the layered rock samples. The first bedding layer represents the weak layer with the inclination angles of 0° (Figure 5a), 30° (Figure 5b), 60° (Figure 5c), and 90° (Figure 5d) with respect to the loading direction. The second layer is the most competent layer containing much higher mechanical strengths related to the weak one. The inclination angle of this layer is also measured from the loading direction and changes (corresponding to the inclination of the first layer) as 90° (Figure 5a), 120° (Figure 5b), 150° (Figure 5c), 180° (Figure 5d), respectively. As shown in these figures (Figures 5 (a-g)), all of the bedding layers are at right angles to one another and three different pairs of thicknesses are chosen for these modelled layers as: 5 mm/10 mm (Figure 5), 10 mm/10 mm (Figure 6), and 20 mm/10 mm (Figure 7). A loading rate of 0.016 m/s is adopted to move the lateral walls of the modelled samples, and the appropriate calibrated micro-properties given in Table 3 are used for the analyses.

Table 3. Micro-properties of weak interface of bedding layer.

Parameter	Low Value	High value	Parameter	Low value	High value
n_bond	1e3	1e6	s_bond	1e3	1e6
fric	0.25	0.5			

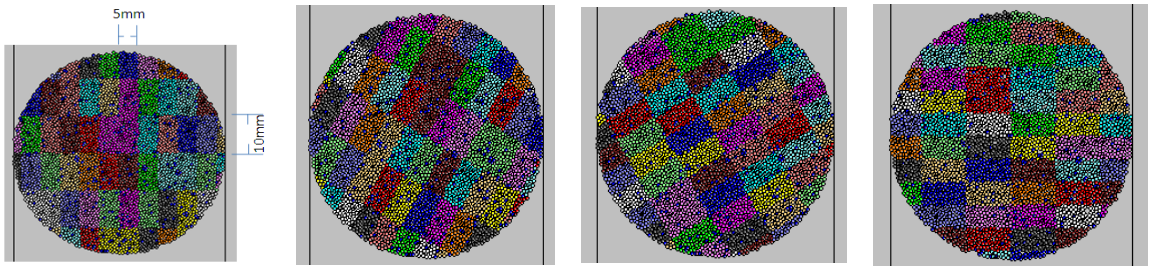

(a) (b) (c) (d)

Figure 5. The models with bedding layers' thicknesses of 5 mm and 10 mm; bedding layers' angle are; a) 0°-90°, b)30°-120°, c) 60°-150°, d) 90°-180°.

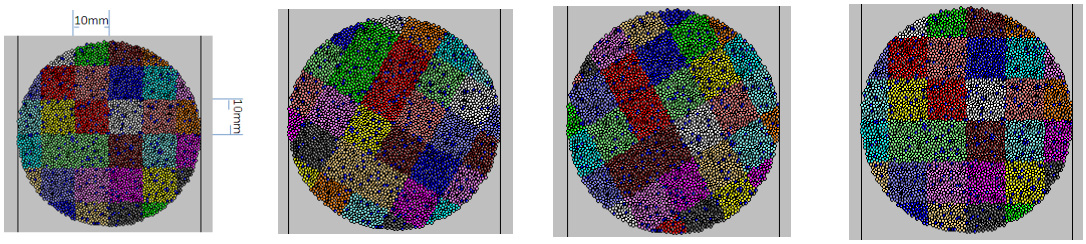

(a) (b) (c) (d)

Figure 6. The models with bedding layers' thicknesses of 10 mm and 10 mm; bedding layers' angle are a) 0°-90°, b) 30°-120°, c) 60°-150°, d) 90°-180°.

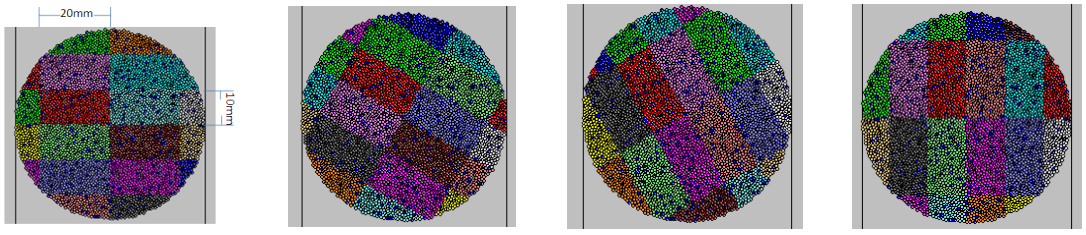

(a) (b) (c) (d)

Figure 7. The models with bedding layers' thicknesses of 20 mm and 10 mm; bedding layers' angle are a) 0°-90°, b) 30°-120°, c) 60°-150°, d) 90°-180°.

3. Effects of transversely Isotropic Bedding Layers on Failure Mechanism of Specimens

The effects of bedding layers' thickness on the failure mechanism of the transversely isotropic geo-material specimens are obtained through the numerical modelling of 3 sets of Brazilian discs containing two layers. There is one weak layer and one competent layer in each disc specimen in which their thicknesses are: 5 mm/10 mm, 10 mm/10 mm and 20 mm/10 mm, respectively.

3.1. Failure mechanism of layers with bedding thickness 5 mm/10 mm

The PFC2D models are analysed to show the effects of the transversely bedding layer on the failure pattern of models for bedding thickness of 5 mm/10 mm, as shown in Figures 8-10. For convenience, the interface angularities of the layers are separately shown in each figure; the yellow lines represent the shear cracks, while the red ones denote the tensile cracks in these figures. The shear cracks are mainly produced in the weak layer while the tensile cracks are more dominant for the competent layer of the specimen. In Figures 8-10, there may be no changes in the inclination angles of the shear cracks as usually occur along the interfaces; on the other hand, the tensile cracks usually occur within the intact part of the layers but mostly in the competent layer of the sample. The branching was increased by increasing the loading rate.

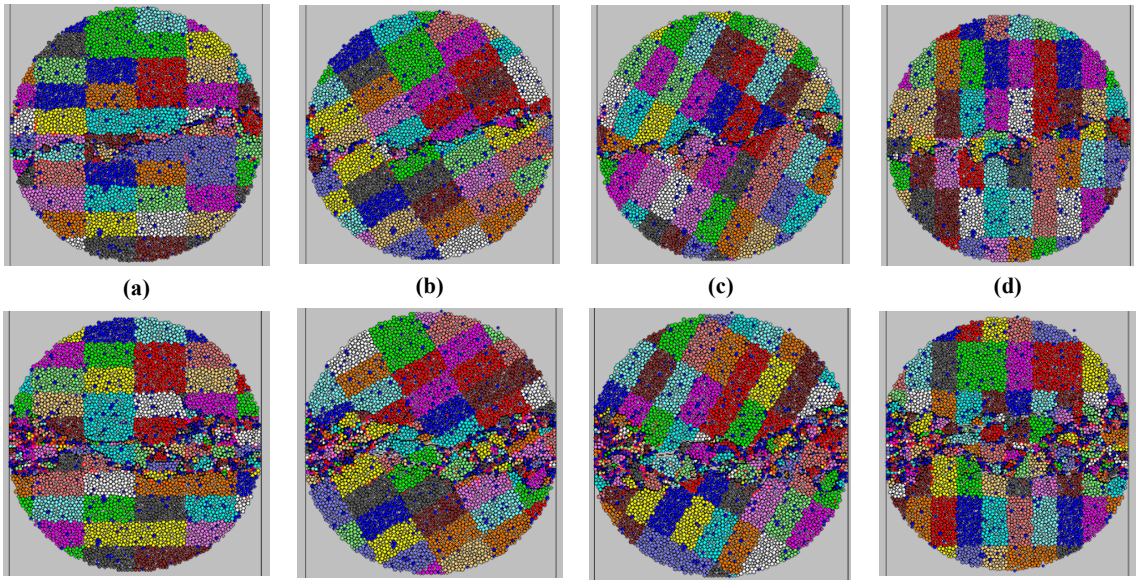

(a) (b) (c) (d)

(e) (f) (g) (h)

Figure 8. Failure pattern of the models with bedding layers' thicknesses of 10 mm and 10 mm; bedding layers' angle are a) 0°-90°, b) 30°-120°, c) 60°-150°, d) 90°-180°, (loading rate = 0.01mm/min), e) 0°-90°, f) 30°-120°, g) 60°-150°, h) 90°-180° (loading rate = 10 mm/min); model diameter = 5 cm.

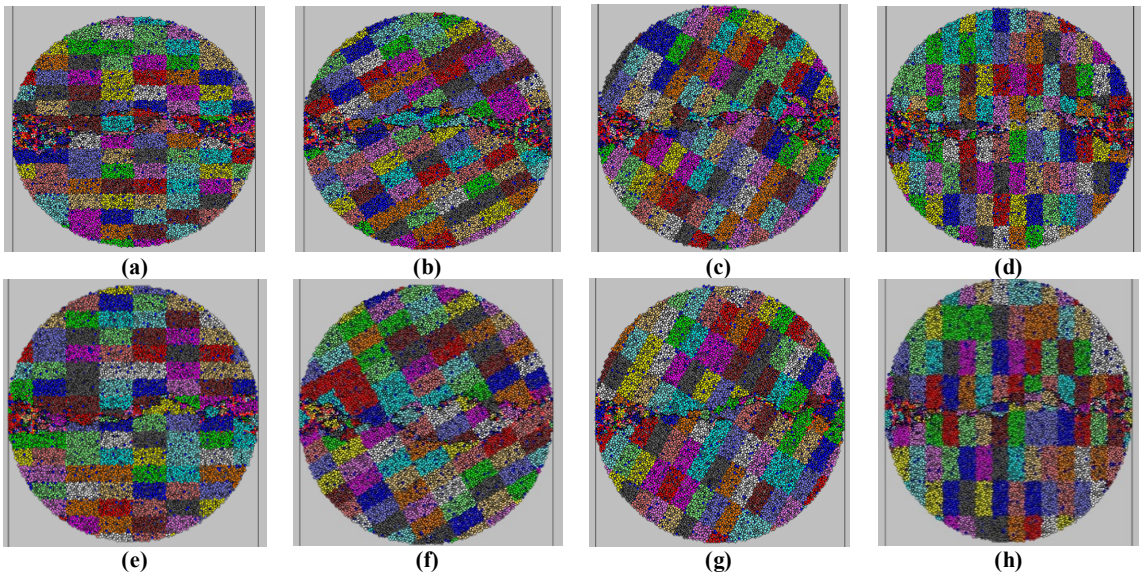

Figure 9. Failure pattern of the models with bedding layers' thicknesses of 10mm and 10 mm; bedding layers' angle are a) 0˚-90˚, b) 30˚-120˚, c) 60˚-150˚, d) 90˚-180˚, (loading rate = 0.01 mm/min), e) 0˚-90˚, f) 30˚-120˚, g) 60˚-150˚, h) 90˚-180˚ (loading rate = 10 mm/min); model diameter = 10 cm.

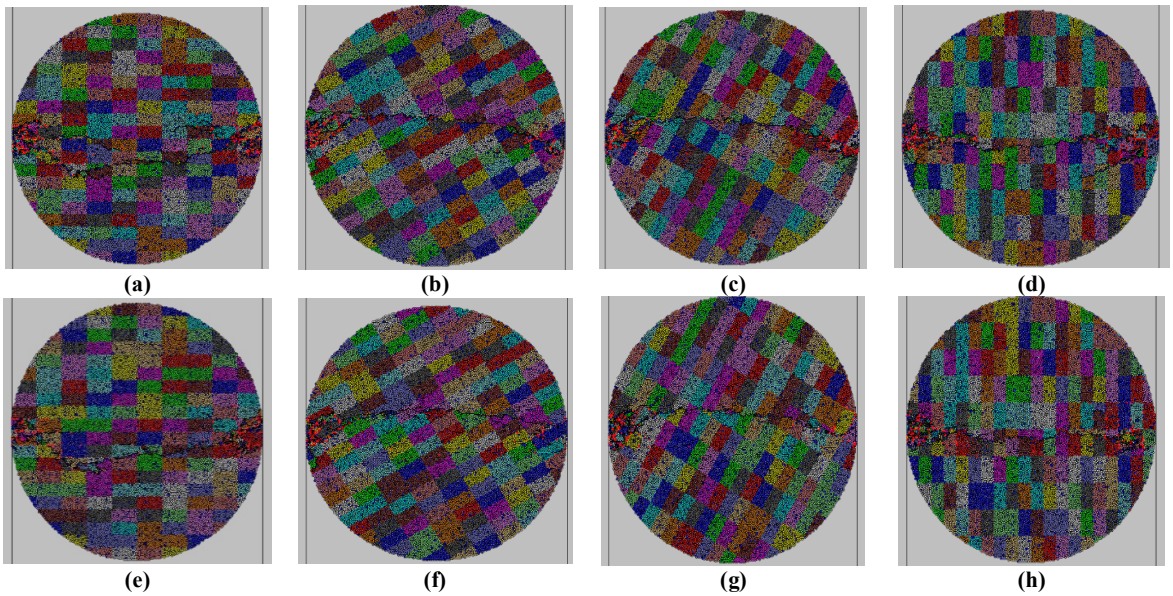

Figure 10. Failure pattern of the models with bedding layers' thicknesses of 10 mm and 10 mm; bedding layers' angle are a) 0˚-90˚, b) 30˚-120˚, c) 60˚-150˚, d) 90˚-180˚, (loading rate = 0.01 mm/min), e) 0˚-90˚, f) 30˚-120˚, g) 60˚-150˚, h) 90˚-180˚ (loading rate = 10 mm/min); model diameter = 15 cm.

3.2. Failure mechanism of layers with bedding thickness 10 mm/10 mm

Figures 11-13 illustrate the effects of the bedding layer on the failure patterns of the PFC2D models for the transversely bedding layers of the rock samples. The thickness of the weak and competent layers in the samples are taken as 10 mm/10 mm, respectively. Effect of various layers' angularities on the failure mechanism of the modelled Brazilian disc samples of the bedded rocks are shown in each figure, where the red lines show the tensile cracks and those of yellow colour represent the shear cracks, which mostly occur in between the layers' interface. The weak layer may cause the shear cracks while the tensile cracks mainly occur in the competent layer especially in its intact part. The branching was increased by increasing the loading rate.

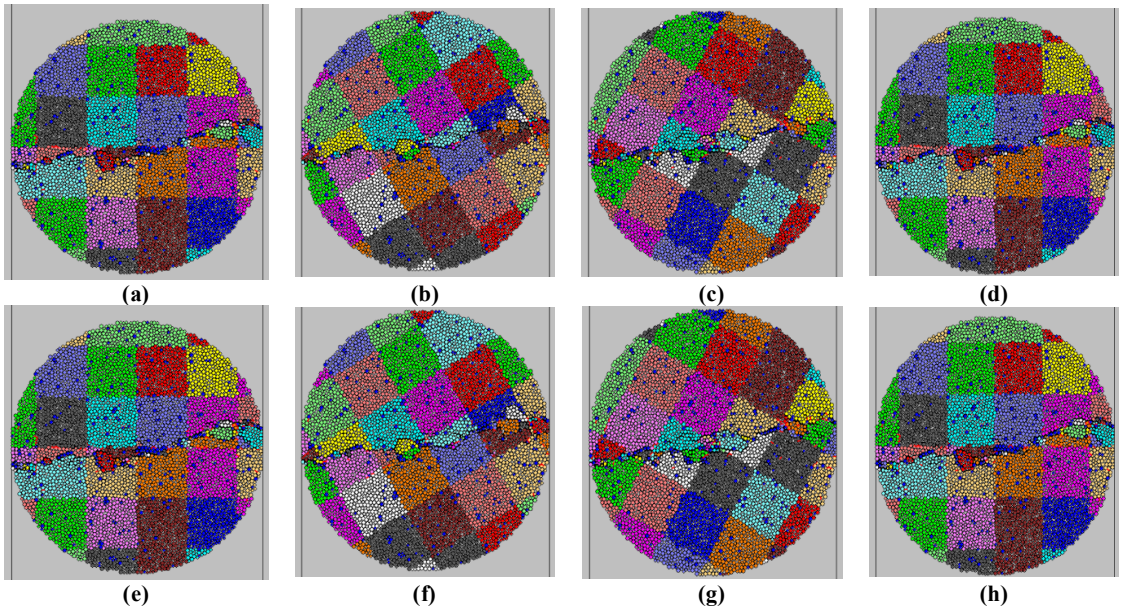

Figure 11. Failure pattern of the models with bedding layers' thicknesses of 10 mm and 10 mm; bedding layers' angle are a) 0°-90°, b) 30°-120°, c) 60°-150°, d) 90°-180°, (loading rate = 0.01 mm/min), e) 0°-90°, f) 30°-120°, g) 60°-150°, h) 90°-180° (loading rate = 10 mm/min); model diameter = 5 cm.

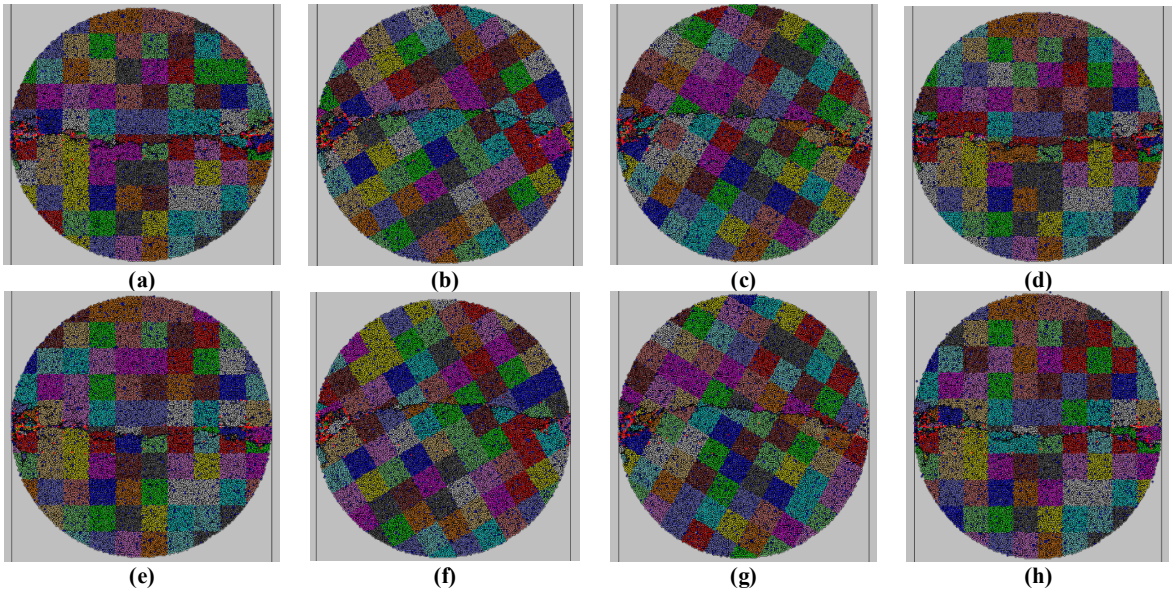

Figure 12. Failure pattern of the models with bedding layers' thicknesses of 10 mm and 10 mm; bedding layers' angle are a) 0°-90°, b) 30°-120°, c) 60°-150°, d) 90°-180°, (loading rate = 0.01 mm/min), e) 0°-90°, f) 30°-120°, g) 60°-150°, h) 90°-180° (loading rate = 10 mm/min); model diameter = 10 cm.

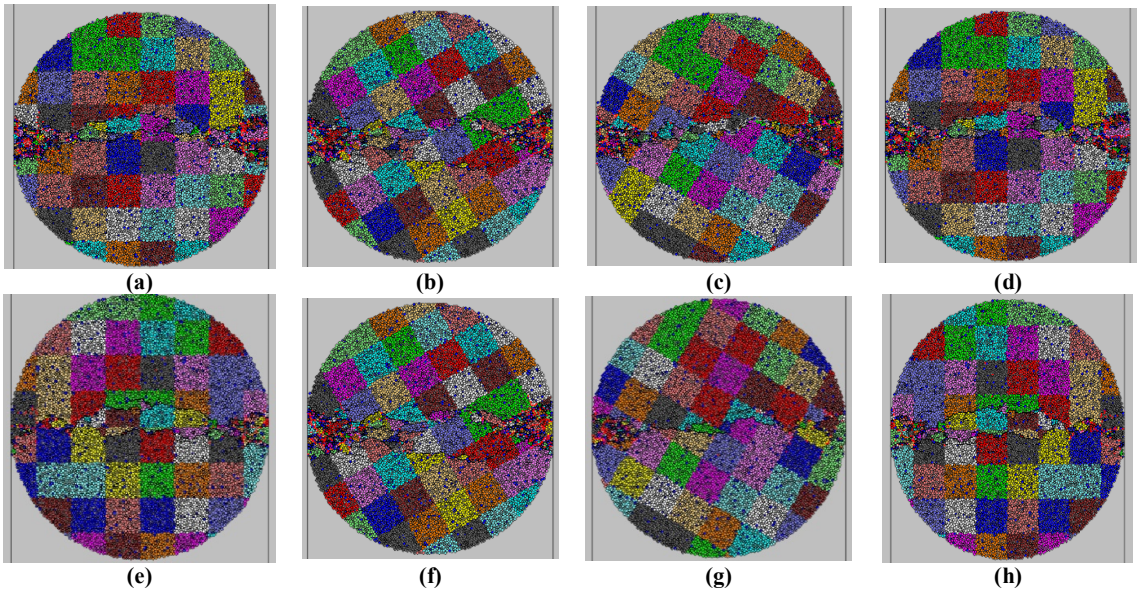

Figure 13. Failure pattern of the models with bedding layers' thicknesses of 10mm and 10 mm; bedding layers' angle are a) 0˚-90˚, b) 30˚-120˚, c) 60˚-150˚, d) 90˚-180˚, (loading rate = 0.01 mm/min), e) 0˚-90˚, f) 30˚-120˚, g) 60˚-150˚, h) 90˚-180˚ (loading rate = 10 mm/min); model diameter = 15 cm.

3.2. Failure mechanism of layers with bedding thickness 20 mm/10 mm

Figures 14-16 show the effects of transversely bedding layer on the failure patterns of the Brazilian disc models for the bedding thicknesses of 20 mm/10 mm (for the weak and competent layers, respectively). In these figures, the results of interfaces angularities for both weak and competent layers have been shown. In all configurations, the yellow and black lines represent the shear and tensile cracks, respectively, and the shear cracks mostly develop in the interfaces between the weaker bedding layers. In this case, the inclination angels of the shear cracks with respect to the normal loading direction changes from 0˚ to 90˚. As a whole, the numbers of shear cracks remains nearly constant as the thickness of the bedding layers' increase. However, for some configuration, as the bedding thickness increases the shear cracks may develop in the layers' interfaces while the tensile cracks usually induce in the intact area of the layers in the model. On the other hand, there may be no failure in the direction of bedding plane interface for the layer of higher strength (competent layer). The branching was increased by increasing the loading rate.

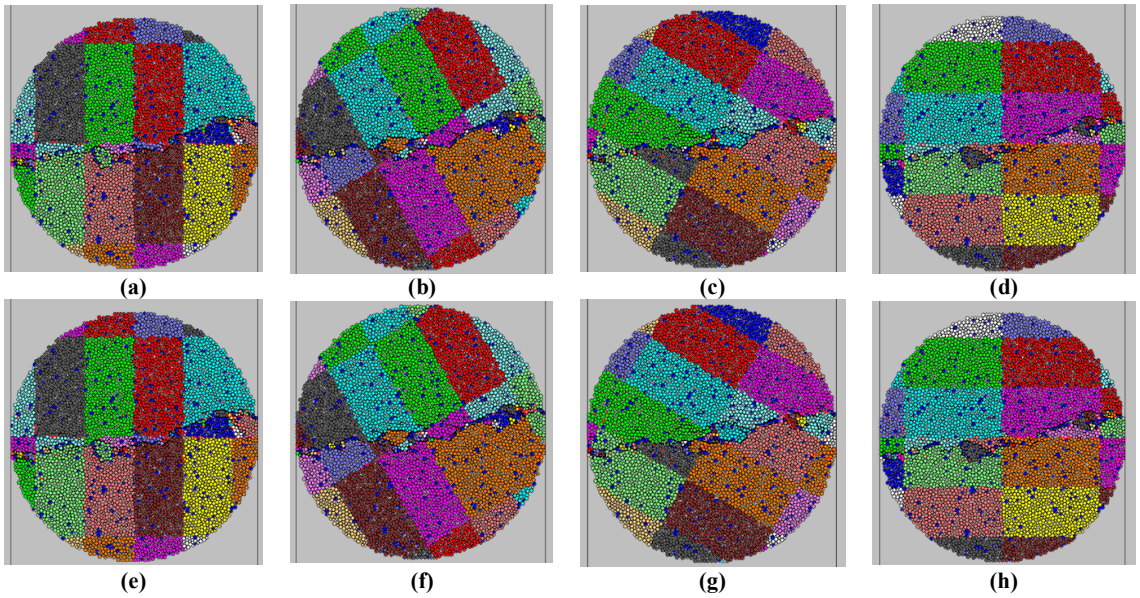

Figure 14. Failure pattern of the models with bedding layers' thicknesses of 10 mm and 10 mm; bedding layers' angle are a) 0˚-90˚, b) 30˚-120˚, c) 60˚-150˚, d) 90˚-180˚, (loading rate = 0.01 mm/min), e) 0˚-90˚, f) 30˚-120˚, g) 60˚-150˚, h) 90˚-180˚ (loading rate = 10 mm/min); model diameter = 5 cm.

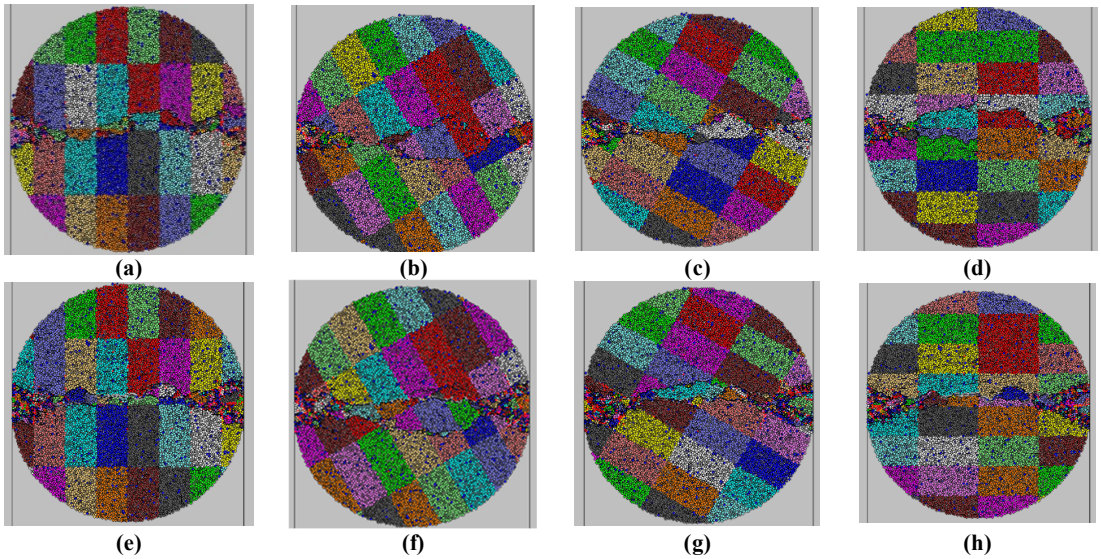

Figure 15. Failure pattern of the models with bedding layers' thicknesses of 10 mm and 10 mm; bedding layers' angle are a) 0˚-90˚, b) 30˚-120˚, c) 60˚-150˚, d) 90˚-180˚, (loading rate = 0.01 mm/min), e) 0˚-90˚, f) 30˚-120˚, g) 60˚-150˚, h) 90˚-180˚ (loading rate = 10 mm/min); model diameter = 5 cm.

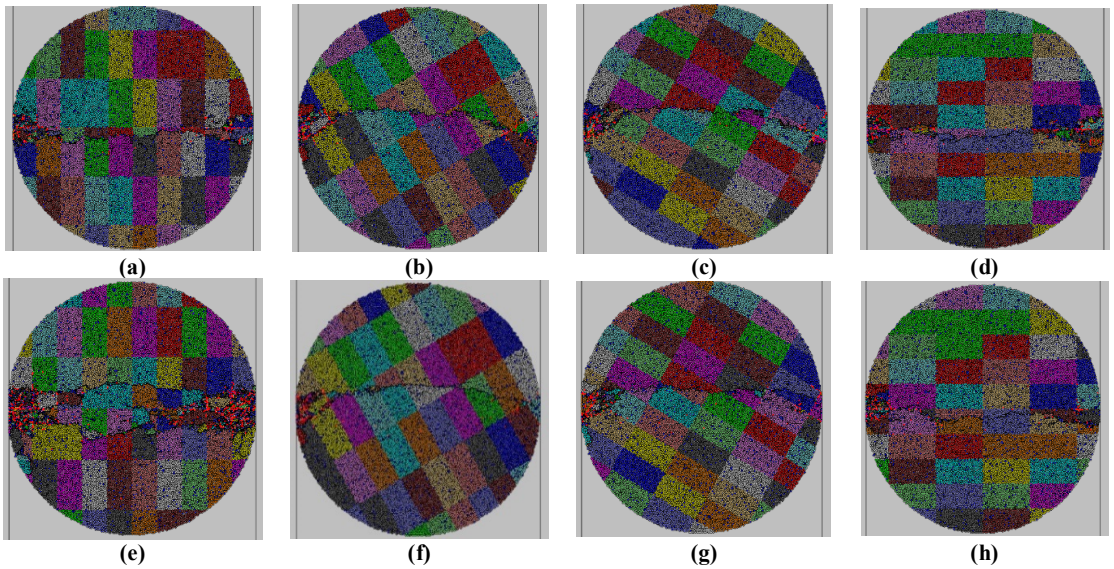

Figure 16. Failure pattern of the models with bedding layers' thicknesses of 10 mm and 10 mm; bedding layers' angle are a) 0°-90°, b) 30°-120°, c) 60°-150°, d) 90°-180°, (loading rate = 0.01 mm/min), e) 0°-90°, f) 30°-120°, g) 60°-150°, h) 90°-180° (loading rate = 10 mm/min); model diameter = 5 cm.

4. Effects of Transversely Bedding Layers on Brazilian Tensile Strength of Specimens

Figure 17 shows the effect of transversely bedding layer on the Brazilian tensile strength for bedding thickness of 5 mm/10 mm, 10 mm/10 mm, and 20 mm/10 mm, respectively. Loading rate was 10 mm/min. In this figure, the results of interfaces angularities have been shown. The minimum Brazilian strength was occurred when weaker interface angle is between the 30° and 60°. The maximum value occurred in 90°. Also, the Brazilian tensile strength was increased by increasing the layer thickness.

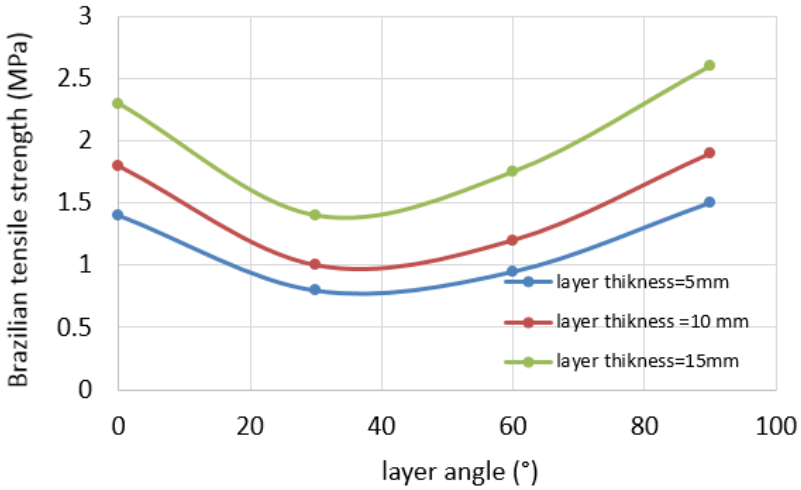

Figure 17. The effect of transversely bedding layer on the Brazilian tensile strength.

Figure 18 shows the effect of modal diameter on the Brazilian tensile strength for bedding thickness of 5 mm/10 mm. In this figure, the results of interfaces angularities have been shown. The minimum Brazilian strength was occurred when weaker interface angle is between the 30° and 60°. The maximum value occurred in 90°. Also, the Brazilian tensile strength was increased by decreasing the model diameter

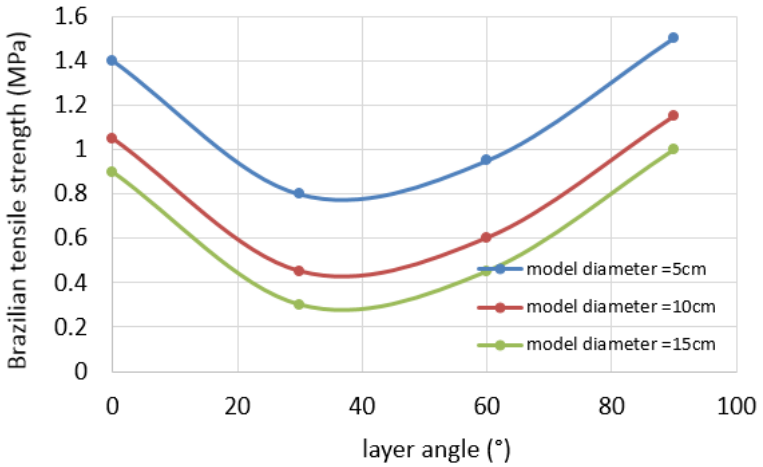

Figure 18. The effect of transversely bedding layer on the Brazilian tensile strength.

Figure 19 shows the effect of transversely bedding layer on the Brazilian tensile strength for bedding thickness of 5 mm/10 mm, 10 mm/10 mm, and 20 mm/10 mm, respectively. Loading rate was 0.01 mm/min. In this figure, the results of interfaces angularities have been shown. The minimum Brazilian strength was occurred when weaker interface angle is between the 30° and 60°. The maximum value occurred in 90°. Also, the Brazilian tensile strength was increased by increasing the layer thickness. By comparison between Figure 19 and Figure 17, it can be concluded that tensile strength was increased by increasing the loading rate.

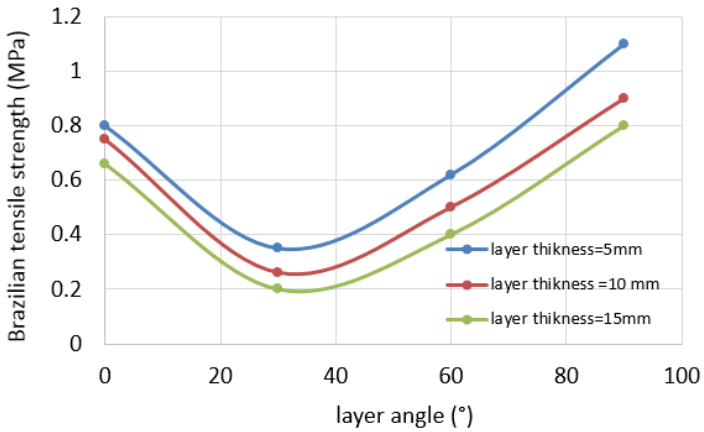

Figure 19. The effect of transversely bedding layer on the Brazilian tensile strength.

From Figures 17-19, By comparison between failure mode and tensile strength, it can be concluded that when a weaker interface angle is between 30° and 60°, pure tensile failure occurred in the model, while shear cracks were observed in interfaces of layers with dip angel of 0° and 90°, whereas the shear strength of rock materials is more than their tensile strength, minimum Brazilian strength occurs when a weaker interface angle is between 30° and 60°. It's to be noted that the tensile strength of the numerical model has a close relationship with layer interfaces. The number of layer interfaces and or weak plane numbers was increased by decreasing the layer thickness, which leads to decreasing the model strength.

5. Discussion

By comparison between the failure behaviour intersected layered rock and failure behaviour of parallel layered rock, it can be concluded that the oriented failure surfaces were occurred in parallel layered rock (Figure 20), while the zigzag cracks occur in intersected layered rock. In other words, the existence of intersected layers having weak mechanical properties change the shear surface direction. The results of this study are in a good accordance with outputs of research done by

kulatilake *et al*. [57]. According to kulatilake *et al*. [57], the intersected weak planes in rock mass changes the failure pattern of rock because intersected weak planes control the crack tearing, crack sliding, and crack splitting (Figure 21).

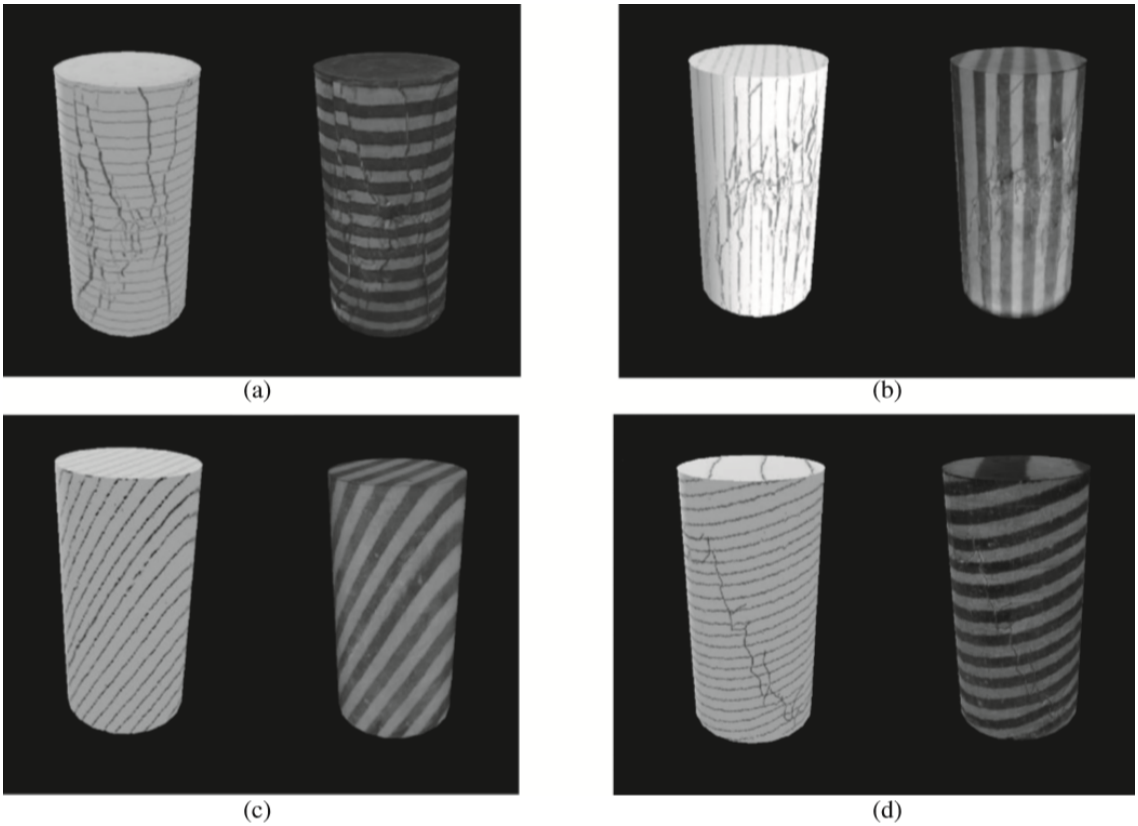

Figure 20. Reconstructed 3-D image of specimens (a) Tensile fracture across discontinuities mode, b) Tensile-split along discontinuities mode, c) Sliding failure along discontinuities mode, d) Sliding failure across discontinuities mode [58].

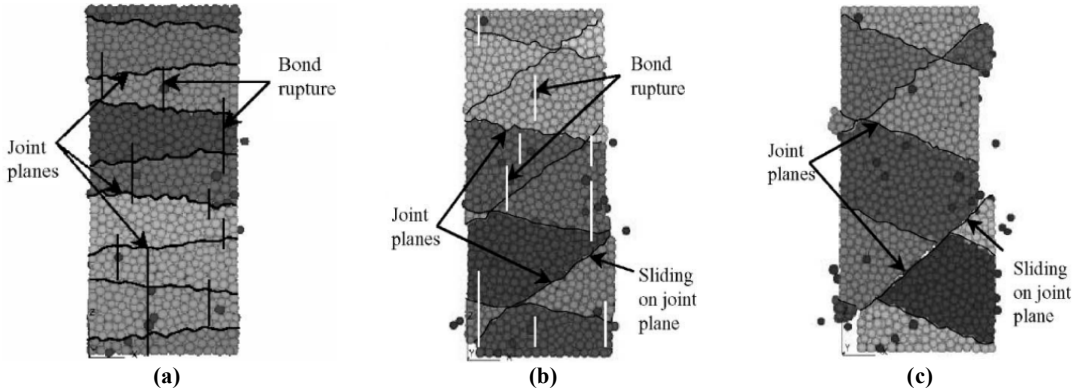

Figure 21. Fractured PFC3D particle assemblies with the three breakage modes obtained from the laboratory and the numerical results (a) Splitting of intact material, (b) Mixed breakage mode, and (c) Sliding breakage [57].

6. Conclusions

In this research work, the failure mechanism of samples with transversely bedding layers were modelled by PFC2D code. Before simulating complex models of transversally bedding layers, uniaxial, Brazilian, and triaxial experimental results are simulated to calibrate the PFC2D code and verify the accuracy of the simulated numerical model response. In this research work, 72 circular

models with a diameter of 54 mm were built. Two bedding layers of weak and strong were considered for the interfaces of the layers. The angles of the first bedding layers were changed from 0° to 90° with an increment of 30°, and the second bedding layers (with high strength) were at right angles to those of weak layers, therefore, changed from 90° to 180°, respectively, with an increment of 15°. Three sets of modelled samples with the change in the first layers' thicknesses were considered (i.e. 5 mm/10 mm, 10 mm/10 mm, and 20 mm/10 mm) in this research work.

The following main conclusions were deduced from these analyses:

- In all of the specimens' configurations, the shear cracks mainly develop in the interfaces and in between the weaker bedding layers.
- The inclination angels of the shear cracks with respect to the applied normal load direction change from 0° to 90° with an increment of 30°.
- Numbers of shear cracks are constant by increasing the bedding layers' and bedding thicknesses.
- In some configuration, the tensile cracks mainly develop in the intact area of material in the model.
- There is not any failure in direction of bedding plane interface considering a layer of high strength (for more competent layers).
- The minimum Brazilian tensile strength of the samples was occurred when the weaker interface angle changed between 30° and 60°, while its maximum value occurred for the interface angle of 90°.
- The Brazilian tensile strength of the samples was increased by increasing the layers' thicknesses.
- The branching was increased by increasing the loading rate.
- The model strength was decreased by increasing the model scale.
- Tensile strength was increased by increasing the loading rate.

References

[1]. Amadei, B. (1996). Importance of anisotropy when estimating and measuring *in situ* stresses in rock. *Int. J. Rock Mech. Min. Sci.* 33, 293–325.

[2]. Jiang, Y., Tanabashi, Y., Li, B., and Xiao, J. (2006). Influence of geometrical distribution of rock joints on deformational behaviour of underground opening. T*unn. Undergr. Space Technol.* 21, 485–491.

[3]. Fortsakis, P., Nikas, K., Marinos, V., and Marinos, P. (2012). Anisotropic behaviour of stratified rock masses in tunnelling. *Eng. Geol.* 141–142, 74–83.

[4]. Xu, T., Ranjith, P.G., Wasantha, P.L.P., Zhao, J., Tang, C.A., and Zhu, W.C. (2013). Influence of the geometry of partially-spanning joints on mechanical properties of rock in uniaxial compression. *Eng. Geol.* 167, 134–147.

[5]. Yu, L., Weetjens, E., Sillen, X., Vietor, T., Li, X., Delage, P., Labiouse, V., and Charlier, R. (2014). Consequences of the thermal transient on the evolution of the damaged zone around a repository for heat-emitting high-level radioactive waste in a clay formation: a performance assessment perspective. *Rock Mech. Rock Eng*. 47, 3–19.

[6]. Wasantha, P.L.P., Ranjith, P.G., Zhang, Q.B., and Xu, T. (2015). Do joint geometrical properties influence the fracturing behaviour of jointed rock? An investigation through joint orientation. J. Geomech. Geophys. *Geol. Energy Geol. Res*. 1, 3–14.

[7]. Li, L.C., Xia, Y.J., Huang, B., Zhang, L.Y., Li, M., and Li, A.S. (2016). The behaviour of fracture growth in sedimentary rocks: a numerical study based on hydraulic fracturing processes. *Energies,* 9, 169–197.

[8]. Johansson, F. (2016). Influence of scale and matedness on the peak shear strength of fresh, unweathered rock joints. *Int. J. Rock Mech. Min.* Sci. 82, 36–47.

[9]. Dan, D.Q. and Konietzky, H. (2014). Numerical simulations and interpretations of Brazilian tensile tests on transversely isotropic rocks. *Int. J. Rock Mech. Min. Sci*. 71, 53–63.

[10]. Duan, K. and Kwok, C.Y. (2015). Discrete element modelling of anisotropic rock under Brazilian test conditions. *Int. J. Rock Mech. Min. Sci*. 78, 46–56.

[11]. Wang, J., Xie, L.Z., Xie, H.P., Ren, L., He, B., Li, C.B., Yang, Z.P., and Gao, C. (2016). Effect of layer orientation on acoustic emission characteristics of anisotropic shale in Brazilian tests. *J. Nat. Gas Sci. Eng*. 36, 1120–1129.

[12]. Wang, P.T., Yang, T.H., Xu, T., Cai, M.F., and Li, C.H. (2016). Numerical analysis on scale effect of elasticity, strength and failure patterns of jointed rock masses. *Geosci. J*. 20, 539–549.

[13]. Wang, T., Xu, D., Elsworth, D., and Zhou, W. (2016). Distinct element modelling of strength variation in jointed rock masses under uniaxial compression. *Geomech. Geophys. Geo-energ. Geo-resour*. 2, 11–24.

[14]. Khosravi, A., Simon, R., and Rivard, P. (2017). The shape effect on the morphology of the fracture surface induced by the Brazilian test. *Int. J. Rock Mech. Min. Sci*. 93, 201–209.

[15]. Xia, K., Yao, W., and Wu, B. (2017). Dynamic rock tensile strengths of Laurentian granite:

experimental observation and micromechanical model. *J. Rock Mech. Geotech. Eng.* 9, 116 -124.

[16]. Yuan, R. and Shen, B. (2017). Numerical modelling of the contact condition of a Brazilian disk test and its influence on the tensile strength of rock. *Int. J. Rock Mech. Min. Sci*. 93, 54–65.

[17]. Zhang, S.W., Shou, K.J., Xian, X.F., Zhou, J.P., and Liu, G.J., 2018. Fractal characteristics and acoustic emission of anisotropic shale in Brazilian tests. *Tunn. Undergr. Space Technol.* 71, 298–308.

[18]. Tien Y.M. and Tsao P.F. (2000). Preparation and mechanical properties of artificial transversely isotropic rock, *Int. J. Rock Mech. Min. Sci.* 37: 1001-1012.

[19]. You S. and Sun J. (2021) bedding plane effects on mechanical behaviour of surrounding rock in mountain tunnelling Shock and Vibration, 2021, Article ID 7346061.

[20]. Wu, W., Wang, G.B., and Mao, H.J. (2010). Investigation of porosity effect on mechanical strength characteristics of dolostone. *Rock Soil Mech.* 31, 3709–3714.

[21]. Cho, J.W., Kim, H., Jeon, S.W., and Min, K.B. (2012). Deformation and strength anisotropy of Asan gneiss, Boryeong shale, and Yeoncheon schist. *Int. J. Rock Mech. Min. Sci.* 50, 158–169.

[22]. Liu, K.D., Liu, Q.S., Zhu, Y.G., and Liu, B. (2013). Experimental study of coal considering directivity effect of bedding plane under Brazilian splitting and uniaxial compression. Chinese *J. Rock Mech. Eng*. 32, 308–316 (in Chinese).

[23]. Dan, D.Q., Konietzky, H., and Herbst, M. (2013). Brazilian tensile strength tests on some anisotropic rocks. *Int. J. Rock Mech. Min. Sci.* 58, 1–7.

[24]. Tavallali, A. and Vervoort, A. (2010). Effect of layer orientation on the failure of layered sandstone under Brazilian test conditions. *Int. J. Rock Mech. Min. Sci.* 47, 313–322.

[25]. Khanlari, G., Rafiei, B., and Abdilor, Y. (2015). An experimental investigation of the Brazilian tensile strength and failure patterns of laminated sandstones. *Rock Mech. Rock Eng.* 48, 843–852.

[26]. Ma, T., Wu, B., Fu, J., Zhang, Q., and Chen, P. (2017). Fracture pressure prediction for layered formations with anisotropic rock strengths. *J. Nat. Gas Sci. Eng*. 38, 485–503.

[27]. Ma, T., Zhang, Q.B., Chen, P., Yang, C., and Zhao, J. (2017). Fracture pressure model for inclined wells in layered formations with anisotropic rock strengths. *J. Petrol. Sci. Eng.* 149, 393–408.

[28]. Min, K.B. and Jing, L.R. (2003). Numerical determination of the equivalent elastic compliance tensor for fractured rock masses using the distinct element method. *Int. J. Rock Mech. Min.* Sci. 40, 795–816.

[29]. Jia, P. and Tang, C.A. (2008). Numerical study on failure mechanism of tunnel in jointed rock mass. *Tunn. Undergr. Space Technol*. 23, 500–507.

[30]. Bahaaddini, M., Hagan, P.C., Mitra, R., and Hebblewhite, B.K. (2014). Scale effect on the shear behaviour of rock joints based on a numerical study. *Eng. Geol.* 181, 212–223.

[31]. Bahaaddini, M., Hagan, P.C., Mitra, R., and Hebblewhite, B.K. (2016). Numerical study of the mechanical behaviour of non-persistent jointed rock masses. *Int. J. Geomech.* 16, 1–10.

[32]. Bahaaddini, M., Hagan, P.C., Mitra, R., and Khosravi, M.H. (2016). Experimental and numerical study of asperity degradation in the direct shear test. *Eng. Geol.* 204, 41–52.

[33]. Zhou, J.R., Wei, J., Yang, T.H., Zhu, W.C., Li, L.C., and Zhang, P.H. (2018). Damage analysis of rock mass coupling joints, water and microseismicity. *Tunn. Undergr. Space Technol*. 71, 366-381.

[34]. Nehrii, S., Nehrii, T., Bachurin, L., and Piskurska, H. (2019). Problems of mining the prospective coal-bearing areas in Donbas. *E3S Web of Conferences*, 123, 01011.

[35]. Nehrii, S., Nehrii, T., Kultaev, S., and Zolotarova, O. (2020). Providing resistance of protection means on the soft adjacent rocks. *E3S Web of Conferences,* 168, 00033.

[36]. Wang, X. W. Y., Yan Y., and Zhang X. (2020). Scale effect of mechanical properties of jointed rock mass: A numerical study based on particle flow code. *Geomechanics and Engineering*, 21(3), 259–268.

[37]. Nehrii S., Nehrii T., Zolotarova O., Aben K., and Yussupov K. (2021). *Determination of the parameters of local reinforced zones under the protection means*. E3S Web of Conferences, 280, 08018.

[38]. Uzun Yaylacı, E., Oner, E., Yaylacı, M., Ozdemir, M. E., Abushattal, A., and Birinci, A. (2022). Application of artificial neural networks in the analysis of the continuous contact problem. *Structural Engineering and Mechanics*, 84(1), 35–48.

[39]. Yaylacı, M., Abanoz, M., Yaylacı, E.U., Ölmez, H., Sekban, D.M., and Birinci, D. (2022), Evaluation of the contact problem of functionally graded layer resting on rigid foundation pressed via rigid punch by analytical and numerical (FEM and MLP) methods. *Arch Appl Mech*., 92, 1953–1971 (2022).

[40]. Özdemir M.E. and Yaylac M. (2023), Research of the impact of material and flow properties on fluid-structure interaction in cage systems, *Wind and Structures*, 36(1):31-40.

[41]. Turan, M., Uzun Yaylacı, E. & Yaylacı, M., (2023), Free vibration and buckling of functionally graded porous beams using analytical, finite element,

and artificial neural network methods. *Arch Appl Mech* 93, 1351–1372 (2023).

[42]. Yaylacı, M., Uzun Yaylacı, E., Ozdemir, M. E., Ozturk, S., and Sesli, H., 2023, Vibration and buckling analyses of FGM beam with edge crack: Finite element and multilayer perceptron methods, *Steel and Composite Structures,* 46, 4, 565-575.

[43]. Golewski G. L. (2023). Mechanical properties and brittleness of concrete made by combined fly ash, silica fume and nanosilica with ordinary Portland cement, *AIMS Materials Science*. 10(3), 390-404.

[44]. Golewski, G.L. (2023). Effect of Coarse Aggregate Grading on Mechanical Parameters and Fracture Toughness of Limestone Concrete, *Infrastructures, 8*, 117.

[45]. Golewski, G.L. (2023). Study of strength and microstructure of a new sustainable concrete incorporating pozzolanic materials, Structural Engineering and Mechanics, *Structural Engineering and Mechanics*, 86 (4): 431-44.

[46]. Golewski, G.L. (2023), Concrete Composites based on Quaternary Blended Cements with a Reduced Width of Initial Microcracks. *Appl. Sci.* 2023, *13*, 7338.

[47]. Golewski, G.L. (2023), The Phenomenon of Cracking in Cement Concretes and Reinforced Concrete Structures: The Mechanism of Cracks Formation, Causes of their Initiation, Types, and Places of Occurrence, and Methods of Detection—A Review. *Buildings*, *13*, 765.

[48]. Li, X.L. (2013). Timodaz: a successful international cooperation project to investigate the thermal impact on the EDZ around a radioactive waste disposal in clay host rocks. *J. Rock Mech. Geotech. Eng*. 5, 231–242.

[49]. Lisjak, A., Garitte, B., Grasselli, G., Müller, H.R., and Vietor, T. (2015). The excavation of a circular tunnel in a bedded argillaceous rock (Opalinus Clay): short-term rock mass response and FDEM numerical analysis. *Tunn. Undergr. Space Technol*. 45, 227–248.

[50]. Wang, S.Y., Sloan, S.W., Tang, C.A., and Zhu, W.C. (2012). Numerical simulation of the failure mechanism of circular tunnels in transversely isotropic rock masses. Tunn. Undergr. Space Technol. 32, 231–244.

[51]. Yang, T.H., Wang, P.T., Xu, T., Yu, Q.L., Zhang, P.H., Shi, W.H., and Hu, G.J. (2015). Anisotropic characteristics of fractured rock mass and a case study in Shirengou Metal Mine in China. *Tunn. Undergr. Space Technol*. 48, 129–139.

[52]. Lazear, G.D. (2009). Fractures, convection and underpressure: hydrogeology on the southern margin of the Piceance basin, *west-central Colorado, USA. Hydrogeol. J*. 17,641–664.

[53]. Gholami, R. and Rasouli, V. (2014). Mechanical and elastic properties of transversely isotropic slate. *Rock Mech. Rock Eng.* 47, 1763–1773.

[54]. Wang, P.T., Ren, F.H., Miao, S.J., Cai, M.F., and Yang, T.H. (2017). Evaluation of the anisotropy and directionality of a jointed rock mass under numerical direct shear tests.

[55]. Itasca. (1999). PFC3D manual, 1st Ed.

[56]. Potyondy, D. O. and Cundall, P. A. (2004). "A bonded-particle model for rock. *Int. J. Rock Mech. Min. Sci*., 41(8), 1329–1364.

[57]. Kulatilake, P.H.S.W., Malama, B., and Wang J. (2001). Physical and particle flow modelling of jointed rock block behaviour under uniaxial loading, *Int. J. Rock Mech. Min.* Sci. 38, 641–657.

[58]. Tien, Y.M., Kuo, M.C., and Lu, Y.C. (2016). Failure criteria for transversely isotropic rock from: Rock Mechanics and Engineering, Volume I: Principles CRC Press.

تجزیه و تحلیل روش المان گسسته دوبعدی ژئومواد الاستیک همسانگرد عرضی بینش در تاثیر مقیاس ها و نرخ بارگذاری

وهاب سرفرازی[۱]، هادی حائری[۲*]، محمد فاتحی[۳]، و غلامرضا سعیدی[۴]

۱. بخش مهندسی معدن، دانشگاه صنعتی همدان، ایران
۲. بخش مهندسی معدن، مجتمع آموزش عالی زرند، دانشگاه شهید باهنر کرمان، ایران
۳. بخش مهندسی معدن و متالورژی، دانشگاه یزد، یزد، ایران
۴. بخش مهندسی معدن، دانشگاه شهید باهنر کرمان، کرمان، ایران

ارسال ۲۰۲۳/۰۸/۳۰، پذیرش ۲۰۲۳/۱۲/۴

* نویسنده مسئول مکاتبات: haerihadi@gmail.com

چکیده:

رفتار مکانیکی سنگ‌های الاستیک همسانگرد عرضی را می‌توان با روش المان گسسته شبیه سازی عددی کرد. لایه‌های بستر متوالی در این سنگ‌ها ممکن است خواص مکانیکی متفاوتی داشته باشند. هدف از این کار پژوهشی بررسی عددی اثر ناهمسانگردی بر رفتار کششی سنگ‌های همسانگرد عرضی است. بنابراین، روش شبیه‌سازی عددی باید با استفاده از آزمایش‌های آزمایشگاهی مرسوم، یعنی آزمون‌های فشاری کششی (برزیلی)، تک محوری و سه محوری به خوبی کالیبره شود. در این مطالعه دو لایه همسانگرد عرضی در ۷۲ مدل دیسکی در نظر گرفته شد. این مدل‌ها با قطر ۵۴ میلی‌متر برای بررسی اثرات ناهمسانگرد لایه‌های بستر بر رفتار مکانیکی ژئومواد شکننده تهیه شدند. همه این لایه‌ها در مدل‌های شبیه‌سازی‌شده به‌طور متقابل عمود بودند، که شامل سه جفت ضخامت ۵ میلی‌متر/۱۰ میلی‌متر، ۱۰ میلی‌متر/۱۰ میلی‌متر و ۲۰ میلی‌متر/۱۰ میلی‌متر بود. سه قطر مختلف برای مدل ها انتخاب شد، یعنی ۵ سانتی متر، ۱۰ سانتی متر و ۱۵ سانتی‌متر. این نمونه‌ها تحت دو نرخ بارگذاری متفاوت، یعنی ۰/۰۱ میلی‌متر در دقیقه و ۱۰ میلی‌متر در دقیقه قرار گرفتند. نتایج به‌دست‌آمده از این مدل‌های شبیه‌سازی شده عددی نشان داد که در لایه‌های ضعیف، ترک‌های برشی با زاویه‌های شیب ۰ تا ۹۰ درجه ایجاد شده‌اند (با در نظر گرفتن افزایش ۱۵ درجه). همچنین با افزایش ضخامت لایه، تغییری در تعداد ترک‌های برشی ایجاد نشد. برخی ترک‌های کششی نیز در مواد دست نخورده مدل‌ها ایجاد شد. در این کار تحقیقاتی هیچ شکستی در صفحه رابط نسبت به لایه با استحکام بالاتر وجود نداشت. انشعاب با افزایش نرخ بارگذاری افزایش یافت. همچنین قدرت مدل با افزایش مقیاس مدل کاهش یافت.

کلمات کلیدی: لایه بستر، صفحه تقاطع، آزمون‌های مقاومت ، المان گسسته، زاویه شیب لایه.